
Variational Phylogenetic Inference with Products over Bipartitions

Evan Sidrow

Department of Statistics and Actuarial Science
Simon Fraser University
Burnaby, Canada
esidrow@sfu.ca

Alexandre Bouchard-Côté

Department of Statistics
University of British Columbia
Vancouver, Canada

Lloyd T. Elliott

Department of Statistics and Actuarial Science
Simon Fraser University
Burnaby, Canada

Abstract

Bayesian phylogenetics requires accurate and efficient approximation of posterior distributions over trees. In this work, we develop a variational Bayesian approach for ultrametric phylogenetic trees. We present a novel variational family based on coalescent times of a single-linkage clustering and derive a closed-form density of the resulting distribution over trees. Unlike existing methods for ultrametric trees, our method performs inference over all of tree space, it does not require any Markov chain Monte Carlo subroutines, and our variational family is differentiable. Through experiments on benchmark genomic datasets and an application to SARS-CoV-2, we demonstrate that our method achieves competitive accuracy while requiring significantly fewer gradient evaluations than existing state-of-the-art techniques.

1 Introduction

The goal of Bayesian phylogenetics is to infer the genealogy of a collection of taxa given a genetic model and aligned sequence data. Phylogenetics is used in fields such as epidemiology (Li et al., 2020), linguistics (List et al., 2014), and ecology (Godoy et al., 2018). Bayesian phylogenetic inference quantifies uncertainty and integrates over phylogenetic tree structures within a phylogenetic model (Zhang and Matsen IV, 2019). Most Bayesian phylogenetic inference is performed using Markov chain Monte Carlo (MCMC) methods with candidate trees iteratively proposed and either accepted or rejected based on their consistency with the observed data. However, MCMC methods can struggle because the number of possible trees grows super-exponentially in the number of taxa and posterior distributions on trees are highly multi-modal.

One alternative to MCMC is variational inference, in which the posterior distribution over phylogenetic tree structures is approximated using a variational distribution that minimizes some distance metric to the true posterior distribution. While variational inference over combinatorial spaces is also known to be difficult due to the complexity of the constraints on the support (Bouchard-Côté and Jordan, 2010; Linderman et al., 2018), there have been several recent advances in variational inference over phylogenetic trees that are tractable. Zhang and Matsen IV (2018) represented phylogenetic trees as Bayesian networks using *subsplit Bayesian networks* (SBNs), and later used SBNs perform variational Bayesian phylogenetic inference on unrooted trees (Zhang and Matsen IV, 2019). This approach has spawned many methodological advancements. To improve the distribution for branch

lengths, Zhang (2020) used normalizing flows, Molén et al. (2024) used mixtures, and Xie et al. (2024) used semi-implicit branch length distributions. To improve the variational family over tree topologies, Zhang (2023) used graph neural networks to learn topological features. However, the number of parameters within an SBN grows exponentially with the number of taxa, so MCMC chains must be used to find the most likely tree structures. To avoid this issue, other recent VI approaches sample tree topologies without the use of SBNs. For example, Koptagel et al. (2022) use a gradient-free variational inference approach and directly sample from the Jukes and Cantor (1969) model, while Mimori and Hamada (2023) use a distance-based metric in hyperbolic space to construct unrooted phylogenetic trees. Further, Zhou et al. (2024) introduce PhylogGFN, a phylogenetic variational inference technique based on reinforcement learning and generative flow networks (Bengio et al., 2023).

In this work we focus on rooted ultrametric phylogenetic trees, where branch lengths correspond to the amount of time between evolutionary branching events. This formulation is useful when time is important, for example in applications involving rapidly evolving pathogens (Sagulenko et al., 2018). However, none of the aforementioned approaches incorporate time constraints into the branch lengths of the phylogenetic trees. To this end, Zhang and Matsen IV (2024) generalized their SBN-based approach to ultrametric trees, but this approach still relies on MCMC chains to restrict a subset of tree space to perform inference over. Alternatively, Bouckaert (2024) outline a method related to the one described in this manuscript. However, because their matrix representation of tree space is not dense, they can only express a limited number of trees. As such, their variational family is not supported on many tree topologies. Further, they do not perform any optimization to find the optimal tree structure and instead rely on empirical values derived from MCMC chains.

To this end, we introduce Variational phylogenetic Inference with **PR**oducts over bipartitions (VIPR), a new variational family for ultrametric trees based on coalescent theory and single-linkage clustering (Kingman, 1982). VIPR naturally performs variational inference on ultrametric trees and thus directly incorporates time into phylogenetic inference. Unlike previous variational methods over ultrametric trees, VIPR performs inference over the entirety of tree space and does not rely on MCMC sub-routines. In particular, we parameterize a variational distribution over a distance matrix and use it to derive a differentiable variational density over trees that result from single-linkage clustering. Through a set of standard experiments and an application to COVID-19, we show that our simple variational formulation achieves comparable results to existing methods for ultrametric trees in fewer gradient evaluations.

2 Background

2.1 Notation

Consider a set of N taxa $\mathcal{X} = \{x_1, x_2, \dots, x_N\}$. A nonempty subset X of \mathcal{X} is referred to as a *clade* of \mathcal{X} . A clade represents a collection of taxa which share a common ancestor at a particular time in the past. Further, we represent evolutionary branching events with bipartitions $\{W, Z\}$ of the clade X .

We focus on *ultrametric trees*, which consist of a rooted, binary tree topology τ and a set of coalescent times $\mathbf{t} = \{t_n\}_{n=1}^{N-1}$, where there is one t_n for each internal node in τ . For ultrametric trees in particular, the branch length between a child and its parent is equal to the difference in coalescent times of the parent and child nodes. We measure \mathbf{t} in backwards time, so each t_n is positive and represents time before present. The leaves of τ correspond to the genomes of each measured taxon $x \in \mathcal{X}$. Additionally, an internal node u of τ represents the (unobserved) genome of the most recent common ancestor of all taxa that have u as a parent node. As a binary tree, τ contains a total of $N - 1$ internal nodes (including the root). We can thus represent the tree with a collection of bipartitions: $\tau = \{\{W_n, Z_n\}\}_{n=1}^{N-1}$. In this representation, an internal node u_n is the most recent common ancestor for all taxa $x \in W_n \cup Z_n$, and the n -th coalescent event is represented by $\{W_n, Z_n\}$.

Denote the set of possible characters within a set of aligned genome sequences by Ω (e.g., a DNA sequence may correspond to $\Omega = \{A, T, C, G\}$ and an RNA sequence to $\Omega = \{A, U, G, C\}$). Further, denote the set of measured genomes by $\mathbf{Y}^{(\text{ob})} = \{Y_1^{(\text{ob})}, \dots, Y_M^{(\text{ob})}\}$, where $Y_m^{(\text{ob})} = (Y_{m,x_1}, \dots, Y_{m,x_N})$ corresponds to the base pairs at site m for all observed taxa $x \in \mathcal{X}$. In addition

to the observed genomes $\mathbf{Y}^{(\text{ob})}$, denote the unobserved genomes of all internal nodes as $\mathbf{Y}^{(\text{un})} = \{Y_1^{(\text{un})}, \dots, Y_M^{(\text{un})}\}$, where $Y_m^{(\text{un})} = (Y_{m,u_1}, \dots, Y_{m,u_{N-1}})$ corresponds the base at site m for all *unobserved* internal nodes u_1, \dots, u_{N-1} . Let the index of the root node be $N - 1$ (so, u_{N-1} is the root node). We denote the combined observed and unobserved genomes by $\mathbf{Y} = \{\mathbf{Y}^{(\text{ob})}, \mathbf{Y}^{(\text{un})}\}$. For further background on phylogenetics, we refer to Hein et al. (2004).

2.2 Phylogenetic Likelihood

For simplicity, we focus on the Jukes and Cantor (1969) model of evolution, but our methods apply more broadly. We define the stationary distribution as π and a 4-by-4 matrix $P(b)$ with entry (i, j) corresponding to the probability of transitioning from base i to base j given branch length b under Jukes and Cantor (1969). The likelihood function of an observed set of genetic sequences $Y^{(\text{ob})}$ at site m is thus:

$$p(Y_m^{(\text{ob})} | \tau, \mathbf{t}) = \sum_{Y_m^{(\text{un})}} \pi(Y_{m,r}) \prod_{(u,v)} (P(b_{u,v}(\tau, \mathbf{t})))_{Y_{m,u}, Y_{m,v}}. \quad (1)$$

Here the product is over all edges (u, v) in τ . As is customary in the phylogenetic inference literature, we assume independence between sites, so the likelihood function for the observed genomes is:

$$p(\mathbf{Y}^{(\text{ob})} | \tau, \mathbf{t}) = \prod_{m=1}^M p(Y_m^{(\text{ob})} | \tau, \mathbf{t}). \quad (2)$$

Equation (2) can be evaluated in $\mathcal{O}(NM)$ time using the pruning algorithm (Felsenstein, 1981), which also is known as the sum-product algorithm (Koller and Friedman, 2009).

2.3 Prior Distribution over Trees

We use the Kingman coalescent (Kingman, 1982) with a constant effective population size N_e as a prior distribution on $p(\tau, \mathbf{t})$:

$$p(\tau, \mathbf{t}) = \frac{2^{N-1}}{N!(N-1)!} \prod_{k=2}^N \lambda_k \exp(-\lambda_k(t_k - t_{k-1})). \quad (3)$$

Here $\lambda_k = \binom{k}{2}/N_e$ is the rate at which taxa coalesce backwards in time.

2.4 Variational Inference for Phylogenetic Trees

Our goal is to infer a posterior distribution over tree structures and coalescent times given the observed genetic sequences:

$$p(\tau, \mathbf{t} | \mathbf{Y}^{(\text{ob})}) = \frac{p(\mathbf{Y}^{(\text{ob})} | \tau, \mathbf{t}) p(\tau, \mathbf{t})}{p(\mathbf{Y}^{(\text{ob})})}. \quad (4)$$

Here $p(\mathbf{Y}^{(\text{ob})})$ is an intractable normalization constant.

Variational inference involves defining a tractable family of probability densities parameterized by some variational parameters ϕ . Then, the posterior density is approximated by a variational density $q_\phi(\tau, \mathbf{t})$ whose parameters ϕ are selected to minimize a divergence measure D between the posterior $p(\cdot, \cdot | \mathbf{Y}^{(\text{ob})})$ and q_ϕ . Here we use the reverse KL divergence:

$$D_{KL}(q_\phi || p) = \mathbb{E}_{(\tau, \mathbf{t}) \sim q_\phi} \left[\log \left(\frac{q_\phi(\tau, \mathbf{t})}{p(\tau, \mathbf{t} | \mathbf{Y}^{(\text{ob})})} \right) \right]. \quad (5)$$

Evaluating the exact posterior $p(\tau, \mathbf{t} | \mathbf{Y}^{(\text{ob})})$ is difficult. Instead, we equivalently (up to a normalizing constant) maximize the evidence lower bound (ELBO), which is also known as the negative variational free energy in statistical physics and some areas of machine learning:

$$\phi^* = \arg \max_{\phi} L(\phi), \quad L(\phi) = \mathbb{E}_{q_{\phi}} \left[\log \left(\frac{p(\tau, \mathbf{t}, \mathbf{Y}^{(\text{ob})})}{q_{\phi}(\tau, \mathbf{t})} \right) \right]. \quad (6)$$

This expectation over q_{ϕ} consists of a sum over tree structures τ and an integral over coalescent times \mathbf{t} , forming the following objective function:

$$L(\phi) = \sum_{\tau} \int_{\mathbf{t}} q_{\phi}(\tau, \mathbf{t}) \log \left(\frac{p(\tau, \mathbf{t}, \mathbf{Y}^{(\text{ob})})}{q_{\phi}(\tau, \mathbf{t})} \right) d\mathbf{t}. \quad (7)$$

Algorithm 1 Single-Linkage Clustering($\mathbf{T}, \mathcal{X}_0$)

- 1: **Input:** Distances $\mathbf{T} \in \mathbb{R}_{>0}^{\binom{N}{2}}$ and taxa set $\mathcal{X}_0 = \{\{x_1\}, \{x_2\}, \dots, \{x_N\}\}$.
 - 2: **for** $n = 1, \dots, N - 1$ **do**
 - 3: $w^*, z^* \leftarrow \arg \min_{w, z} \{t^{\{w, z\}} : w, z \text{ not coalesced}\}$.
 - 4: Set $W_n \in \mathcal{X}_0$ as the set containing w^* .
 - 5: Set $Z_n \in \mathcal{X}_0$ as the set containing z^* .
 - 6: $t_n \leftarrow t^{\{w^*, z^*\}}$
 - 7: Remove W_n, Z_n from \mathcal{X}_0 and add $W_n \cup Z_n$ to \mathcal{X}_0 .
 - 8: **end for**
 - 9: $\tau \leftarrow \{\{W_n, Z_n\}\}_{n=1}^{N-1}$
 - 10: $\mathbf{t} \leftarrow \{t_n\}_{n=1}^{N-1}$
 - 11: **Return** (τ, \mathbf{t})
-

2.5 Matrix Representation of Tree Space

One way to construct a phylogenetic tree is to use a distance matrix \mathbf{T} (a symmetric $N \times N$ matrix with positive and finite off-diagonal entries) and the *single-linkage clustering* algorithm, as described in Algorithm 1. We denote the distance between taxa u and v by $t^{\{u, v\}}$ and formulate the algorithm to return a representation of a phylogenetic tree using bipartitions and coalescent times that is consistent with our notation. We consider the distance matrix as an element of $\mathbb{R}_{>0}^{\binom{N}{2}}$ by identifying the off-diagonal elements. Algorithm 1 is a naive implementation of single-linkage clustering with time complexity $\mathcal{O}(N^3)$ and space complexity $\mathcal{O}(N^2)$. Sibson (1973) introduce SLINK, an implementation with time complexity $\mathcal{O}(N^2)$ and space complexity $\mathcal{O}(N)$, and prove that both are optimal.

Bouckaert (2024) use single-linkage clustering to perform variational inference over ultrametric trees. First, they note that if exactly $N - 1$ entries of \mathbf{T} are finite, then single-linkage clustering implies a bijection between \mathbf{T} and (τ, \mathbf{t}) . Then, they specify exactly $N - 1$ entries of \mathbf{T} to be random and finite, setting all other entries to infinity. Next, they run an MCMC algorithm over trees to obtain an empirical distribution over coalescent times. Finally, they estimate the parameters associated with the $N - 1$ finite entries of \mathbf{T} using the MCMC-generated empirical distribution. This method has several notable setbacks. First, all entries of \mathbf{T} must be specified to specify a distribution over all of tree space. Further, it is unclear how to select the $N - 1$ best entries of \mathbf{T} to cover the most posterior probability. To correct these issues, we present a gradient-based variational inference method for ultrametric trees based on single-linkage clustering that specifies a variational distribution over all of tree space.

3 Methods

We now present our method **Variational phylogenetic Inference with PRoducts** over bipartitions (VIPR). We begin by outlining a generative process for sampling from our variational distribution q_{ϕ} . We then describe how to evaluate the density of our variational distribution. Finally, we describe the optimization procedure used to maximize our variational objective function.

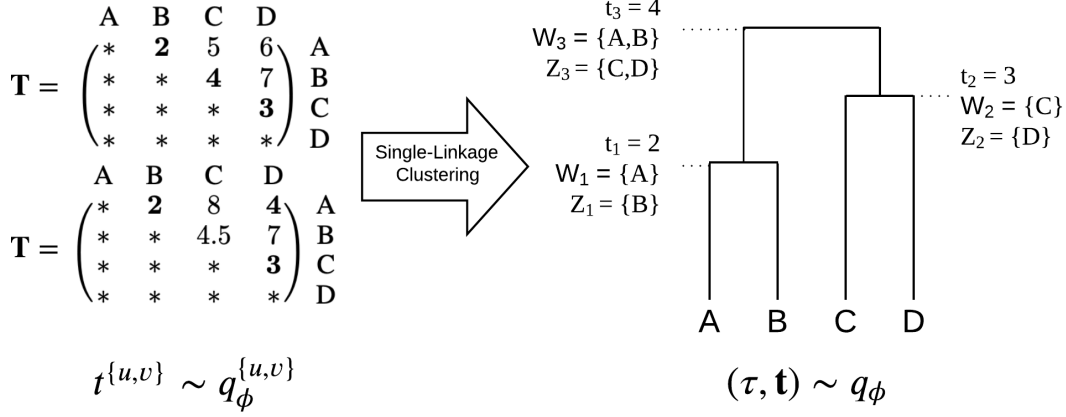


Figure 1: **Diagram of the sampling process for VIPR.** Two possible example matrices \mathbf{T} could be drawn using $t^{\{u,v\}} \sim q_\phi^{\{u,v\}}$ and result in the same phylogenetic tree $(\tau, \mathbf{t}) \sim q_\phi$ after single-linkage clustering. Entries of \mathbf{T} that trigger a coalescence event are shown in bold. The form of $q_\phi^{\{u,v\}}$ is defined by the practitioner, while the expression for q_ϕ depends upon $q_\phi^{\{u,v\}}$ and is defined in Equation (8).

3.1 Generative Process for Phylogenies

We begin by describing a generative process for sampling from q_ϕ , as our variational distribution is best understood by an algorithm for sampling from it. Our algorithm to sample an ultrametric tree with leaf vertices \mathcal{X} proceeds similarly to Algorithm 1 of Bouckaert (2024). Namely, we randomly draw each element of the distance matrix \mathbf{T} ($t^{\{u,v\}}$ for all $\{u, v\} \subset \mathcal{X}$) using a set of independent variational distributions with densities $q_\phi^{\{u,v\}}$. Then, we run single linkage clustering on \mathbf{T} to form (τ, \mathbf{t}) .

Note that $q_\phi^{\{u,v\}}(t^{\{u,v\}})$ and $q_\phi(\tau, \mathbf{t})$ are closely related: $q_\phi^{\{u,v\}}$ describes the distribution over entry $t^{\{u,v\}}$ of \mathbf{T} , while q_ϕ describes the distribution over phylogenetic trees (τ, \mathbf{t}) formed by running single-linkage clustering on \mathbf{T} . Algorithm 2 presents pseudocode to sample from q_ϕ if $q_\phi^{\{u,v\}}$ is a log-normal distribution. Figure 1 visualizes the process of drawing \mathbf{T} using $t^{\{u,v\}} \sim q_\phi^{\{u,v\}}$ and then using single-linkage clustering to map \mathbf{T} to (τ, \mathbf{t}) .

Algorithm 2 Sample- $q(\mu, \sigma, \mathcal{X})$

- 1: **Input:** Parameters $\mu \in \mathbb{R}^{\binom{N}{2}}$ and $\sigma \in \mathbb{R}_{>0}^{\binom{N}{2}}$.
- 2: Draw $z^{\{u,v\}} \sim \mathcal{N}(0, 1)$ for all $\{u, v\} \subset \mathcal{X}$
- 3: Define matrix $\mathbf{T} \in \mathbb{R}_{>0}^{\binom{N}{2}}$ such that:

$$\log(t^{\{u,v\}}) = \mu^{\{u,v\}} + z^{\{u,v\}} \sigma^{\{u,v\}}$$

- 4: **Return** Single-Linkage Clustering(\mathbf{T}, \mathcal{X})
-

3.2 Density Evaluation

While Algorithm 2 presents a straightforward way to sample from the variational distribution, *a priori* it is unclear how to evaluate the variational density q_ϕ of a tree generated from Algorithm 2. This is because a given tree (τ, \mathbf{t}) may have been generated from multiple distance matrices \mathbf{T} (see Figure 1). Remarkably, this sampling procedure yields a density with a closed-form solution, as shown in Proposition 1 below.

Proposition 1. *If the random variables $t^{\{u,v\}}$ are mutually independent, all $q_\phi^{\{u,v\}}$ are continuous in ϕ and \mathbf{t} for all $u, v \in \mathcal{X}$, and $Q_\phi^{\{u,v\}}$ is the survival function of $t^{\{u,v\}}$, then $q_\phi(\tau, \mathbf{t})$ has the following form:*

$$q_\phi(\tau, \mathbf{t}) = \prod_{n=1}^{N-1} \left(\left(\sum_{\substack{w \in W_n \\ z \in Z_n}} \frac{q_\phi^{\{w,z\}}(t_n)}{Q_\phi^{\{w,z\}}(t_n)} \right) \left(\prod_{\substack{w \in W_n \\ z \in Z_n}} Q_\phi^{\{w,z\}}(t_n) \right) \right). \quad (8)$$

A derivation of Proposition 1 using induction is provided in Appendix A. Every taxa pair $\{u, v\}$ appears in the sum and product terms of Equation (8) exactly once, as each taxa pair coalesces exactly once within a rooted phylogenetic tree. Thus, evaluating both $q_\phi(\tau, \mathbf{t})$ and $\nabla_\phi \log q_\phi(\tau, \mathbf{t})$ takes $\mathcal{O}(N^2)$ time.

If $q_\phi^{\{u,v\}}$ is continuously differentiable, then q_ϕ is also continuously differentiable. In our VIPR implementation, $q_\phi^{\{u,v\}}$ is log-normal. We can thus compute gradients with respect to ϕ . Note however that Proposition 1 holds for any continuous mutually independent $q_\phi^{\{u,v\}}$.

We now have almost everything we need to perform phylogenetic variational inference: an (unnormalized) phylogenetic posterior density $p(\tau, \mathbf{t}, \mathbf{Y}^{(\text{ob})})$, a variational family with density $q_\phi(\tau, \mathbf{t})$, and an objective function $L(\phi)$ to maximize in order to find a variational posterior distribution. However, as shown in Algorithm 3, optimizing $L(\phi)$ with stochastic gradient methods such as Adam (Robbins and Monro, 1951; Kingma and Ba, 2014) requires random estimates of the gradient $\nabla_\phi L(\phi)$. Thus, in the following section we consider three methods for gradient estimation: leave-one-out REINFORCE (Mnih and Gregor, 2014; Shi et al., 2022), the reparameterization trick (Kingma and Welling, 2014), and VIMCO (Mnih and Rezende, 2016).

Algorithm 3 $\text{VIPR}(\phi, \mathcal{X}, K)$

- 1: Initialize variational parameters ϕ
 - 2: **while** not converged **do**
 - 3: **for** $k = 1, \dots, K$ **do**
 - 4: Draw $\mathbf{T}^{(k)} \in \mathbb{R}_{>0}^{\binom{N}{2}}$ with $t^{\{u,v\}} \sim q_\phi^{\{u,v\}}$
 - 5: $(\tau^{(k)}, \mathbf{t}^{(k)}) \leftarrow \text{Single-Linkage Clustering}(\mathbf{T}^{(k)}, \mathcal{X})$
 - 6: **end for**
 - 7: Estimate gradient $\nabla_\phi L(\phi)$ using $(\tau^{(k)}, \mathbf{t}^{(k)})$ for $k = 1, \dots, K$.
 - 8: Update ϕ using gradient estimates and a stochastic optimization algorithm (Adam, SGD, etc.)
 - 9: **end while**
 - 10: **Return** ϕ
-

3.3 Gradient Estimators for q_ϕ

3.3.1 The REINFORCE Estimator

Define $f_\phi(\tau, \mathbf{t}) \equiv \log(p(\tau, \mathbf{t}, \mathbf{Y}^{(\text{ob})})) - \log(q_\phi(\tau, \mathbf{t}))$, so that $L(\phi) = \mathbb{E}_{q_\phi}[f_\phi(\tau, \mathbf{t})]$. We can interchange the gradients and the finite sum over τ due to the linearity of integrals. Further, for any fixed τ , under standard regularity conditions (L’Ecuyer, 1995), we can interchange the gradient and the integral from Equation (7). After performing some algebra, we obtain the *leave-one-out REINFORCE* (LOOR) estimator (Mnih and Gregor, 2014; Shi et al., 2022). See Appendix C for the precise formulation.

3.3.2 The Reparameterization Trick

The push out estimator (Rubinstein, 1992), popularized in the machine learning literature under the name of the *reparameterization trick* (Kingma and Welling, 2014), is also included in our numerical experiments when $q_\phi^{\{u,v\}}$ is a log-normal distribution for all $u, v \in \mathcal{X}$. In Algorithm 2, the candidate

coalescent times $t^{\{u,v\}} \sim \text{Lognormal}(\mu^{\{u,v\}}, \sigma^{\{u,v\}}) \iff t^{\{u,v\}} = \exp(\mu^{\{u,v\}} + \sigma^{\{u,v\}} z^{\{u,v\}})$ with $z^{\{u,v\}} \sim \mathcal{N}(0, 1)$. Thus, we approximate the gradient $\nabla_{\phi} L(\phi)$ as

$$\nabla_{\phi} L(\phi) \approx \frac{1}{K} \sum_{k=1}^K \nabla_{\phi} \log \left(\frac{p(\mathbf{Y}, g_{\phi}(\mathbf{Z}^{(k)}))}{q_{\phi}(g_{\phi}(\mathbf{Z}^{(k)}))} \right) \quad (9)$$

$$\mathbf{Z}^{(k)} \sim \mathcal{N}(\cdot; \mathbf{0}, I). \quad (10)$$

Where $g_{\phi}(\mathbf{Z}) = \text{Single-Linkage Clustering}(\exp(\boldsymbol{\mu} + \boldsymbol{\sigma} \odot \mathbf{Z}), \mathcal{X})$ and $\mathcal{N}(\cdot; \mathbf{0}, I)$ is a $\binom{N}{2}$ -dimensional standard normal. The gradient in Equation (9) can be found using automatic differentiation in libraries such as PyTorch (Paszke et al., 2019). This gradient approximation is biased because the interchange of the integral and gradient implied by Equation (9) is not valid in this setting (see Appendix C). Because this estimator is biased, standard results on convergence of stochastic gradient do not hold. Nonetheless, in practice we find that these gradient estimates perform well.

3.3.3 The VIMCO Estimator

One drawback of the single-sample ELBO in Equation (6) is that variational distributions that target the ELBO tend to be mode-seeking (*i.e.*, they can underestimate variance of the true posterior). As an alternative, Mnih and Rezende (2016) suggest a K -sample ELBO that encourages mode-covering behaviour in the posterior:

$$L_K(\phi) = \mathbb{E}_{q_{\phi}} \left[\log \left(\frac{1}{K} \sum_{i=1}^K \frac{p(\tau^{(k)}, \mathbf{t}^{(k)}, \mathbf{Y}^{(\text{ob})})}{q_{\phi}(\tau^{(k)}, \mathbf{t}^{(k)})} \right) \right]. \quad (11)$$

Here, $(\tau^{(k)}, \mathbf{t}^{(k)}) \sim q_{\phi}$ for $k = 1, \dots, K$. This is the objective function used by Zhang and Matsen IV (2024) to perform VBPI. When using this objective function, the VIMCO estimator is an analogous gradient estimator to the LOOR estimator for the single-sample ELBO. See Appendix C for the precise definition of the VIMCO estimator.

4 Experiments

We compared the performance of our VIPR methods with that of Zhang and Matsen IV 2024 (denoted VBPI in this section). We studied eleven commonly used genetic datasets that are listed in Lakner et al. (2008) denoted DS1 through DS11 (these are the names that are given to these datasets in Lakner et al. 2008).

We also studied a dataset of 72 COVID-19 genomes obtained from GISAID (Global Initiative on Sharing All Influenza Data; Khare et al. 2021). In particular, we obtained COVID-19 RNA sequences collected in Canada on January 2, 2025; submitted to GISAID prior to January 20, 2025; containing at least 29,000 sequenced base pairs; and of the strain JN.1. The 72 COVID-19 genomes studied here are all of the COVID-19 genomes provided by GISAID that satisfied all of these criteria. After obtaining these genomes, we aligned them using multiple sequence alignment in MAFFT using the FFT-NS-1 algorithm (Kato and Standley, 2013). Finally, we subset the genomes to $M = 3101$ non-homologous sites (*i.e.*, we omit all sites that are the same across all 72 taxa). The final datasets range from 27 – 72 total taxa N and 378 – 3101 total sites M .

For all methods considered (BEAST, VBPI and our VIPR methods), we used a Kingman coalescent prior on the phylogenies. We fixed the effective population size at $N_e = 5$ (Kingman, 1982) and assumed the Jukes-Cantor model for mutation (Jukes and Cantor, 1969). These assumptions are summarized above in Sections 2.2 and 2.3. We also measured the branch lengths in terms of expected mutations per site, which is in line with BEAST and VBPI.

Each run for the experiments on the DS1 to DS11 datasets was executed on a supercomputer node. The runs were allocated 12 hours of wallclock time, 1 CPU, and 16GB of RAM. The supercomputer had a heterogeneous infrastructure involving in which each CPU make and model was Intel v4 Broadwell, Intel Cascade Lake or Skylake, or AMD EPYC 7302. Experiments on the COVID-19 dataset were run with identical conditions to those for DS1 to DS11, but without the 12 hour limit on wallclock time. Instead, they were run for 10,000 iterations (*i.e.*, parameter updates) or 12 hours (whichever took longer).

4.1 The BEAST Gold Standard

To approximate the true posterior distribution of each dataset we ran 10 independent MCMC chains using BEAST, each with 10,000,000 iterations. We discarded the first 250,000 iterations as burn-in and thinned to every 1,000-th iteration. This yielded in a total of 97,500 trees that were used as a “gold standard”. We estimated ground-truth marginal log-likelihood values using the stepping-stone estimator (Xie et al., 2010). For each dataset, we ran 100 path steps of 500,000 MCMC iterations and repeated this process ten times to obtain 10 independent estimates of the marginal log-likelihood.

4.2 The VBPI Baseline

The VBPI baseline requires MCMC runs to determine likely subsplits (*i.e.*, evolutionary branching events). To provide these runs, we used BEAST to obtain a rooted subsplit support. We ran 10 independent MCMC chains for 1,000,000 iterations, with the first 250,000 discarded as burn-in. We then thinned to every 1,000-th iteration, yielding 7,500 trees for the VBPI subsplit support. To fit the VBPI baseline, we used the VIMCO gradient estimator with K -sample ELBO for $K = 10$ and $K = 20$ (indicated by VBPI10 and VBPI20 in our plots and tables below). We used the Adam optimization algorithm implemented in PyTorch with four random restarts and learning rates of 0.003, 0.001, 0.0003, and 0.0001 (Kingma and Ba, 2014; Paszke et al., 2019). We estimated the marginal log-likelihood every 100 iterations (*i.e.*, parameter updates) using 500 importance-sampled particles. Of the 16 runs for each VBPI batch size condition (4 learning rates and 4 random restarts), we retained the run with the highest average MLL in the last 10 estimates of the run. This run (with highest average MLL) is included in our plots and figures. We used the primary subsplit pair (PSP) parameterization of VBPI. Code for these experiments was adapted from <https://github.com/zcrabbit/vbpi>. See Zhang and Matsen IV (2024) for more implementation details.

4.3 The VIPR Methods

For our VIPR methods, we set the variational distributions $q_{\phi}^{\{u,v\}}$ to be log-normal, so the variational parameters ϕ were the means and standard deviations corresponding to the logarithm of the entries $\log(t^{\{u,v\}})$ of the matrix \mathbf{T} . To initialize the parameters ϕ , we computed the empirical distribution of coalescent times between taxa $\{u, v\}$ from the short MCMC runs used to establish the support for the VBPI baseline. We then set the initial mean and standard deviation of $q_{\phi}^{\{u,v\}}$ to be the mean and standard deviation of the empirical distribution. We experimented with three gradient estimation techniques. We estimated $\nabla_{\phi} L(\phi)$ using (1) the LOOR estimator and (2) the reparameterization trick, both with batch sizes of 10 samples. We also estimated $\nabla_{\phi} L_K(\phi)$ using the VIMCO estimator with a batch size of $K = 10$. For each gradient estimation technique, we used the Adam optimizer in PyTorch with ten random restarts and learning rates of 0.001, 0.003, 0.01, and 0.03. We recorded the estimated marginal log-likelihood every 10 iterations (*i.e.*, parameter updates) with 50 Monte Carlo samples. Of the 40 runs (4 learning rates and 10 random restarts), we retained the run with the highest average MLL in the last 10 estimates of the run. As for VBPI, the retained run (for each dataset and technique) is reported in the plots and figures below.

5 Results

Tables 1 and 2 show the estimated marginal log-likelihoods (MLLs) and ELBOs for our variational inference experiments after 12 hours of compute time. The stepping-stone algorithm is not a variational method, so it has no entry in Table 2. The marginal log-likelihoods in Table 1 are reported by the gap between the MLL of the gold standard (BEAST/stepping stone run) and the method’s MLL (the difference between the MLLs). So, methods with smaller gaps are closer to the gold standard, and the method with the highest MLL is bolded. Note that some VI methods surpass the gold standard, likely due to Monte Carlo error.

VBPI tends to slightly outperform our VIPR methods in terms of MLL, but all methods are comparable in terms ELBO (with our methods outperforming VBPI on approximately half of the datasets). This is likely because VBPI directly targets the multi-sample ELBO for optimization, which produces mode-covering behaviour. In contrast, our VIPR methods target the single-sample ELBO.

Table 1: *Gap between gold standard and estimated marginal log-likelihoods for variational inference methods (in nats)*. Marginal log-likelihoods for VI methods were estimated using importance sampling with 1,000 random samples from each variational distribution. Values indicate differences between gold standard MLL and each method’s MLL. Gold standard MLLs (indicated by the BEAST column) are derived from 10 independent chains of the stepping-stone algorithm in BEAST. Datasets (DATA column) DS1 to DS11 are from Lakner et al. (2008). Dataset COV is the COVID-19 dataset obtained from GISAID. VI methods are specified by columns: Variational Bayesian Phylogenetic Inference with K -sample ELBO, $K = 10, 20$ (VBPI10 and VBPI20; Zhang and Matsen IV 2024); VIPR using the leave-one-out REINFORCE estimator (LOOR); VIPR using the reparameterization trick (REP); VIPR using the Variational Inference for Monte Carlo Objectives estimator with $K = 10$ (VIMCO).

DATA	(N, M)	BEAST	VBPI10	VBPI20	LOOR	REP	VIMCO
DS1	(27, 1949)	-7154.26(0.19)	-0.53(0.09)	0.36(0.13)	-2.29(0.15)	-1.83(0.21)	-0.95(0.46)
DS2	(29, 2520)	-26566.42(0.26)	0.16(0.24)	0.01(0.20)	-0.76(0.14)	-0.14(0.43)	-0.37(0.29)
DS3	(36, 1812)	-33787.62(0.36)	-0.44(0.12)	-0.38(0.13)	-3.66(0.53)	-1.91(0.99)	-2.63(0.50)
DS4	(41, 1137)	-13506.05(0.32)	0.03(0.53)	0.46(0.43)	-2.48(0.43)	-0.47(1.21)	-1.73(0.23)
DS5	(50, 378)	-8271.26(0.39)	-1.70(0.35)	-5.69(0.48)	-0.29(1.82)	-4.01(0.28)	0.94(2.08)
DS6	(50, 1133)	-6745.31(0.55)	-0.76(0.20)	-0.32(0.35)	-3.96(0.34)	-3.26(0.60)	-2.72(0.37)
DS7	(59, 1824)	-37323.88(0.66)	0.27(0.26)	-0.24(0.17)	-2.73(0.30)	-2.82(0.31)	-10.42(0.70)
DS8	(64, 1008)	-8650.20(0.77)	-0.82(0.27)	0.47(0.64)	-3.28(0.99)	-4.95(0.47)	-2.88(0.60)
DS9	(67, 955)	-4072.66(0.53)	-5.32(0.31)	-4.12(0.46)	-3.12(1.21)	-5.79(0.74)	-7.60(0.44)
DS10	(67, 1098)	-10102.65(0.65)	-0.88(0.20)	-1.44(0.22)	-5.38(0.42)	-3.98(1.14)	-6.82(0.49)
DS11	(71, 1082)	-6272.57(0.68)	-18.79(0.41)	-16.28(0.46)	-6.79(0.89)	-7.31(0.71)	-9.62(1.46)
COV	(72, 3101)	-7861.61(0.74)	-39.08(0.58)	-33.26(0.76)	-611.84(1.80)	-374.62(0.48)	-214.25(0.42)

Table 2: *Estimated evidence lower bounds for variational inference methods (in nats)*. ELBOs were estimated using importance sampling on 1,000 random samples from each variational distribution. Our VIPR methods beat the VBPI baseline on half of the datasets. Dataset names, method acronyms, and conditions match Table 1.

DATA	(N, M)	VBPI10	VBPI20	LOOR	REP	VIMCO
DS1	(27, 1949)	-7157.99(0.15)	-7158.18(0.16)	-7159.56(0.10)	-7159.54(0.09)	-7161.60(0.20)
DS2	(29, 2520)	-26573.03(0.28)	-26573.60(0.30)	-26569.56(0.06)	-26569.50(0.08)	-26570.74(0.13)
DS3	(36, 1812)	-33793.96(0.20)	-33794.75(0.28)	-33794.96(0.08)	-33794.77(0.07)	-33796.53(0.15)
DS4	(41, 1137)	-13541.39(13.12)	-13613.68(22.18)	-13512.54(0.11)	-13512.60(0.11)	-13513.41(0.14)
DS5	(50, 378)	-8281.03(0.26)	-8298.64(5.97)	-8279.93(0.11)	-8280.35(0.11)	-8282.03(0.17)
DS6	(50, 1133)	-6751.77(0.22)	-6752.60(0.21)	-6754.36(0.12)	-6755.29(0.14)	-6756.10(0.21)
DS7	(59, 1824)	-37331.12(0.22)	-37331.82(0.31)	-37333.36(0.19)	-37332.04(0.14)	-37352.10(0.42)
DS8	(64, 1008)	-8657.78(0.30)	-8658.83(0.22)	-8662.26(0.16)	-8661.88(0.16)	-8664.54(0.26)
DS9	(67, 955)	-4088.64(0.39)	-4091.21(0.52)	-4085.61(0.18)	-4087.25(0.20)	-4090.52(0.22)
DS10	(67, 1098)	-10111.81(0.29)	-10112.80(0.28)	-10114.76(0.15)	-10115.16(0.16)	-10119.70(0.26)
DS11	(71, 1082)	-6329.37(9.90)	-6559.24(54.99)	-6289.60(0.17)	-6289.70(0.18)	-6294.31(0.20)
COV	(72, 3101)	-8100.96(109.62)	-7913.84(0.93)	-8489.82(0.21)	-8244.41(0.21)	-8087.43(0.30)

Figures 2 and 3 show the trace of estimated log-likelihood vs iteration number for all VI methods on DS1 (Figure 2) and on the COVID-19 dataset (Figure 3). See Appendix B for results on DS2-11. These figures also display empirical distributions of tree metrics for each VI method’s learned variational distribution in addition to the BEAST gold standard run (plotted with matplotlib’s *kde* function with default parameters, Hunter 2007). We removed 2 of the 1,000 trees sampled from VBPI20 for the COVID-19 experiment because they had extremely low log-likelihood ($< -90,000$), resulting in flat densities.

VIPR tended to underestimate the variance of tree length compared to BEAST, while VBPI tended to overestimate. In addition, the reinforce and reparameterization gradient estimates result in variational distributions with higher tree log-likelihoods on average, while VBPI and our VIPR with VIMCO tend to produce trees with more variable log-likelihood values. Again, this behaviour is consistent with the idea that the multi-sample ELBO tends to produce mode-covering variational distributions. VIPR converged quickly on DS1 because the parameters were initialized in a region of high ELBO. However, convergence was slower for the COVID-19 dataset, and the parameters were initialized with low ELBO. This may be because the optimization was caught in relatively flat regions of the parameter space. This highlights the need for intelligent parameter initializations or annealing schedules.

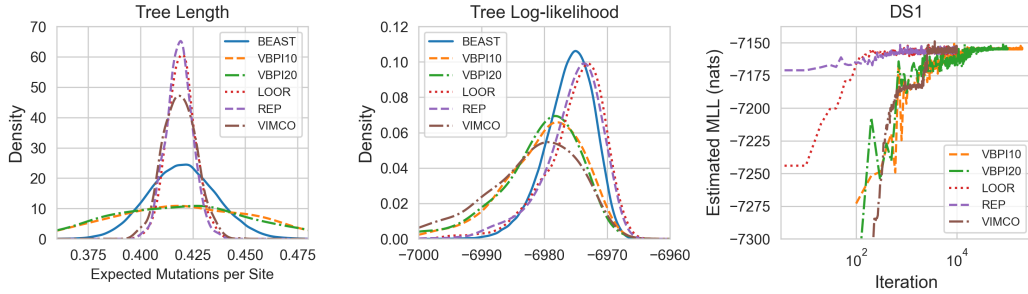


Figure 2: **Variational inference results for dataset DS1.** left: Density estimation for tree lengths. center: Density estimation for tree log-likelihoods. Estimates are formed from 1,000 samples from the variational posterior of each VI method and 97,500 samples from the BEAST gold standard. right: Trace plot of estimated marginal log-likelihood vs. iteration number (i.e., parameter update). Marginal log-likelihood was estimated using 500 importance samples for VBPI and 50 importance samples for VIPR methods.

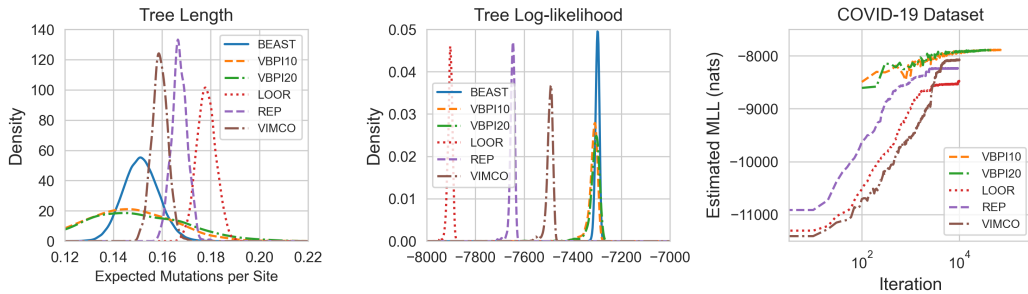


Figure 3: **Variational inference results for the COVID-19 dataset.** left: Density estimation for tree lengths. center: Density estimation for tree log-likelihoods. right: Trace plot of estimated marginal log-likelihood vs. iteration number (i.e., parameter update). Density estimation was performed in the same way as in Figure 2.

5.1 Computational Complexity

To compare the time complexity of our algorithm against VBPI, we used the COVID-19 dataset (with 72 genomes), ran 1,000 iterations of each VI method (VBPI and the three VIPR methods), and recorded the average wallclock time per gradient evaluation. We then subset the COVID-19 dataset by randomly selecting 48, 24, 12, 6, and 3 taxa and repeated this procedure to find computation cost as a function of number of taxa (the same random selection was used for each method). We plot the change in the logarithm of the wallclock time versus the logarithm of the number of taxa in Figure 4. The y-axis corresponds to the computational complexity of the algorithm (e.g., a y-value of 2 corresponds to a time complexity of $\mathcal{O}(N^2)$). This experiment supports that VIPR has an empirical time complexity roughly on the order of N^2 . The VBPI method also appears to have a similar empirical scaling. Zhang and Matsen IV (2024) show that the gradient calculation for their variational family has linear complexity with respect to the number of parameters, but we conjecture that the number of parameters may grow super-linearly with the number of taxa N .

6 Discussion

In this work, we introduce a new variational family over ultrametric, time-measured phylogenies that models the coalescent time between each pair of taxa. The family is formed by deriving a closed-form expression for the marginal distribution on phylogenies induced by single linkage clustering of a distance matrix.

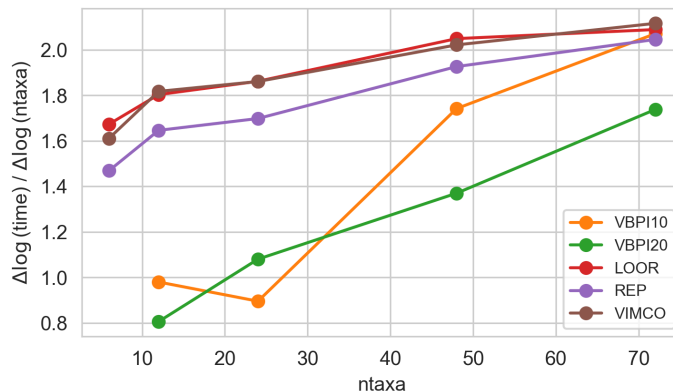


Figure 4: *Slope of the logarithm of seconds-per-iteration vs. the logarithm of the number of taxa.* Each VI method was run for 1,000 iterations on subsets of the COVID-19 dataset. The y-axis corresponds to the computational complexity of the algorithm as a function of number of taxa (i.e., 1 corresponds to linear complexity, 2 corresponds to quadratic complexity, etc.)

Methods using this variational family require only $\mathcal{O}\binom{N}{2}$ parameters in total, and each parameter has an intuitive interpretation as a description of the distribution on pairwise coalescents. For example, in this work we place independent log-normal distributions on the entries of the distance matrix, yielding $2\binom{N}{2}$ parameters (one mean and one standard deviation for each pair of taxa).

Our methods may be further developed in many ways. For example, by moving from the log-normal distribution on pairwise coalescent times to mixture distributions similar to Molén et al. (2024), or normalizing flows similar to Zhang (2020). We could also directly enforce sparsity in the prior by fixing the distribution on the time to coalescence of taxa u and v (when u and v are far away in genetic space) at infinity, further reducing the number of parameters to learn.

Expanding the variational family to include conditional parameters may also improve performance: if taxa u and v are the first to coalesce, we could define a new parameter $\phi^{\{u,v\},w}$ describing the coalesce between a clade containing $\{u, v\}$ and another taxon w .

Our variational inference for phylogenetics is unique in that it does not require aspects of MCMC runs in its iterations in order to make inference computationally tractable. (In contrast, in Zhang and Matsen IV 2024 for example MCMC is used to fix the support of the trees described by their variational family). Note however that we did use short MCMC runs to initialize the parameters of our log-normal distributions.

Fast and accurate parameter initializations and well-tuned annealing are essential for top performance in variational Bayesian phylogenetics. Our experiments may be improved by using an annealing schedule similar to Zhang and Matsen IV (2024) during optimization to prevent convergence to local maxima.

We have focused on the difficult task of inferring tree topology and branch lengths. However, inference for aspects such as a relaxed clock (see Douglas et al., 2021) and the effective populations size N_e can also be done starting from this new variational family. Our method thus serves as a promising foundation on which more intricate inference can be built.

Acknowledgements

We gratefully acknowledge all data contributors, i.e., the Authors and their Originating laboratories responsible for obtaining the specimens, and their Submitting laboratories for generating the genetic sequence and metadata and sharing via the GISAID Initiative, on which this research is based. This research was enabled in part by support provided by the Digital Research Alliance of Canada.

References

- Bengio, Y., Lahlou, S., Deleu, T., Hu, E. J., Tiwari, M., and Bengio, E. (2023). Gflownet foundations. *Journal of Machine Learning Research*, 24(210):1–55.
- Bouchard-Côté, A. and Jordan, M. I. (2010). Variational inference over combinatorial spaces. In *Advances in Neural Information Processing Systems 23*.
- Bouckaert, R. R. (2024). Variational Bayesian phylogenies through matrix representation of tree space. *PeerJ*, 12:e17276.
- Douglas, J., Zhang, R., and Bouckaert, R. R. (2021). Adaptive dating and fast proposals: Revisiting the phylogenetic relaxed clock model. *PLOS Computational Biology*, 17(2):1–30.
- Felsenstein, J. (1981). Evolutionary trees from DNA sequences: a maximum likelihood approach. *J Mol Evol*, 17(6):368–378.
- Godoy, B. S., Camargos, L. M., and Lodi, S. (2018). When phylogeny and ecology meet: Modeling the occurrence of Trichoptera with environmental and phylogenetic data. *Ecology and Evolution*, 8(11):5313–5322.
- Hein, J., Schierup, M., and Wiuf, C. (2004). *Gene genealogies, variation and evolution: a primer in coalescent theory*. Oxford University Press, USA.
- Hunter, J. D. (2007). Matplotlib: A 2d graphics environment. *Computing in Science & Engineering*, 9(3):90–95.
- Jukes, T. H. and Cantor, C. R. (1969). Chapter 24 - evolution of protein molecules. In *Mammalian Protein Metabolism*, pages 21–132. Academic Press.
- Katoh, K. and Standley, D. M. (2013). MAFFT multiple sequence alignment software version 7: improvements in performance and usability. *Mol. Biol. Evol.*, 30(4):772–780.
- Khare, S., Gurry, C., Freitas, L., Schultz, M. B., Bach, G., Diallo, A., Akite, N., Ho, J., Lee, R. T., Yeo, W., GISAI Core Curation Team, and Maurer-Stroh, S. (2021). GISAI’s role in pandemic response. *China CDC Weekly*, 3(49):1049–1051.
- Kingma, D. and Welling, M. (2014). Autoencoding variational Bayes. In *Proceedings of the Second International Conference on Learning Representations*.
- Kingma, D. P. and Ba, J. (2014). Adam: A method for stochastic optimization. *CoRR*, abs/1412.6980.
- Kingman, J. (1982). The coalescent. *Stochastic Processes and their Applications*, 13(3):235–248.
- Koller, D. and Friedman, N. (2009). *Probabilistic Graphical Models: Principles and Techniques - Adaptive Computation and Machine Learning*. The MIT Press.
- Koptagel, H., Kviman, O., Melin, H., Safinianaini, N., and Lagergren, J. (2022). Vaiphy: a variational inference based algorithm for phylogeny. In *Advances in Neural Information Processing Systems 36*.
- Lakner, C., van der Mark, P., Huelsenbeck, J. P., Larget, B., and Ronquist, F. (2008). Efficiency of Markov chain Monte Carlo tree proposals in Bayesian phylogenetics. *Systematic Biology*, 57(1):86–103.
- L’Ecuyer, P. (1995). On the interchange of derivative and expectation for likelihood ratio derivative estimators. *Management Science*, 41(4):738–748.
- Li, T., Liu, D., and Yang, Y. (2020). Phylogenetic supertree reveals detailed evolution of SARS-CoV-2. *Scientific Reports*, 10, 22366.
- Linderman, S., Mena, G., Cooper, H., Paninski, L., and Cunningham, J. (2018). Reparameterizing the Birkhoff polytope for variational permutation inference. In *Proceedings of the Twenty-First International Conference on Artificial Intelligence and Statistics*.

- List, J., Nelson-Sathi, S., Geisler, H., and Martin, W. (2014). Networks of lexical borrowing and lateral gene transfer in language and genome evolution. *Bioessays*, 36(2):141–150.
- Maclaurin, D., Duvenaud, D., and Adams, R. P. (2015). Autograd: Effortless gradients in numpy. In *ICML 2015 AutoML Workshop*.
- Mimori, T. and Hamada, M. (2023). GeoPhy: Differentiable phylogenetic inference via geometric gradients of tree topologies. In *Advances in Neural Information Processing Systems 37*.
- Mnih, A. and Gregor, K. (2014). Neural variational inference and learning in belief networks. In *Proceedings of the 31st International Conference on Machine Learning*.
- Mnih, A. and Rezende, D. (2016). Variational inference for Monte Carlo objectives. In *Proceedings of the 33rd International Conference on Machine Learning*, pages 1791–1799.
- Molén, R., Kviman, O., and Lagergren, J. (2024). Improved variational Bayesian phylogenetic inference using mixtures. *Transactions on Machine Learning Research*.
- Paszke, A., Gross, S., Massa, F., Lerer, A., Bradbury, J., Chanan, G., Killeen, T., Lin, Z., Gimelshein, N., Antiga, L., Desmaison, A., Kopf, A., Yang, E., DeVito, Z., Raison, M., Tejani, A., Chilamkurthy, S., Steiner, B., Fang, L., Bai, J., and Chintala, S. (2019). PyTorch: An imperative style, high-performance deep learning library. In *Advances in Neural Information Processing Systems 32*.
- Robbins, H. and Monro, S. (1951). A Stochastic Approximation Method. *The Annals of Mathematical Statistics*, 22(3):400 – 407.
- Rubinstein, R. Y. (1992). Sensitivity analysis of discrete event systems by the ‘push out’ method. *Annals of Operations Research*, 39(1):229–250.
- Sagulenko, P., Puller, V., and Neher, R. A. (2018). TreeTime: Maximum-likelihood phylodynamic analysis. *Virus Evol.*, 4(1).
- Shi, J., Zhou, Y., Hwang, J., Titsias, M., and Mackey, L. (2022). Gradient estimation with discrete Stein operators. In *Advances in Neural Information Processing Systems 35*.
- Sibson, R. (1973). Slink: An optimally efficient algorithm for the single-link cluster method. *The Computer Journal*, 16(1):30–34.
- Xie, T., Matsen IV, F. A., Suchard, M. A., and Zhang, C. (2024). Variational Bayesian phylogenetic inference with semi-implicit branch length distributions. *arXiv preprint arXiv:2408.05058*.
- Xie, W., Lewis, P. O., Fan, Y., Kuo, L., and Chen, M.-H. (2010). Improving marginal likelihood estimation for Bayesian phylogenetic model selection. *Systematic Biology*, 60(2):150–160.
- Zhang, C. (2020). Improved variational Bayesian phylogenetic inference with normalizing flows. In *Advances in Neural Information Processing Systems 33*.
- Zhang, C. (2023). Learnable topological features for phylogenetic inference via graph neural networks. In *Proceedings of the Eleventh International Conference on Learning Representations*.
- Zhang, C. and Matsen IV, F. A. (2018). Generalizing tree probability estimation via Bayesian networks. In Bengio, S., Wallach, H., Larochelle, H., Grauman, K., Cesa-Bianchi, N., and Garnett, R., editors, *Advances in Neural Information Processing Systems 31*. Curran Associates, Inc.
- Zhang, C. and Matsen IV, F. A. (2019). Variational Bayesian phylogenetic inference. In *Proceedings of the Seventh International Conference on Learning Representations*.
- Zhang, C. and Matsen IV, F. A. (2024). A variational approach to Bayesian phylogenetic inference. *Journal of Machine Learning Research*, 25(145):1–56.
- Zhou, M. Y., Yan, Z., Layne, E., Malkin, N., Zhang, D., Jain, M., Blanchette, M., and Bengio, Y. (2024). PhyloGFN: Phylogenetic inference with generative flow networks. In *The Twelfth International Conference on Learning Representations*.

Appendices for Variational Phylogenetic Inference with Products over Bipartitions

Appendix A: Proof for Proposition 1

We provide a proof by induction for the derivation of equation (8). Consider the coalescent events in algorithm 2. For $1 \leq K \leq N - 1$, Let $\mathbf{t}_{1:K}$ be the times of the first K coalescent events ($\mathbf{t}_{1:K} = \{t_n\}_{n=1}^K$). Let $\tau_{1:K}$ be the bipartitions of the first K coalescent events ($\tau_{1:K} = \{\{W_n, Z_n\}\}_{n=1}^K$). Let $q_{\phi,K}(\tau_K, \mathbf{t}_K)$ be the probability density function of the marginal distribution on the times and bipartitions of the first K coalescent events. Let \mathcal{S}_n be the set $\{\{w, z\} : w \in W_n, z \in Z_n\}$ (here $\{W_n, Z_n\}$ is the n -th bipartition). Note that \mathcal{S}_n is the set of all unordered pairs of taxa that have not coalesced before t_n and that coalesce at t_n . Let $\mathcal{S}_{1:K}$ be $\bigcup_{n=1}^K \mathcal{S}_n$ (i.e., $\mathcal{S}_{1:K}$ is the set of all unordered pairs of taxa that coalesce by time t_n).

By the definition of \mathcal{S}_n , a sum $\sum_{w \in W_n, z \in Z_n}$, is equal to the same sum indexed by \mathcal{S}_n . (And the same is true of products.)

Our induction hypothesis for $1 \leq K \leq N - 1$ is as follows:

$$q_{\phi,K}(\tau_{1:K}, \mathbf{t}_{1:K}) = \prod_{n=1}^K \left(\left(\sum_{\{w,z\} \in \mathcal{S}_n} \frac{q_{\phi}^{\{w,z\}}(t_n)}{Q_{\phi}^{\{w,z\}}(t_n)} \right) \prod_{\{w,z\} \in \mathcal{S}_n} Q_{\phi}^{\{w,z\}}(t_n) \right) \prod_{\{w,z\} \notin \mathcal{S}_{1:K}} Q_{\phi}^{\{w,z\}}(t_K). \quad (12)$$

In (12), the product over $\{w, z\} \notin \mathcal{S}_{1:K}$ is outside of the product over $n = 1, \dots, K$. (Throughout this derivation, if a product sign has more than one factor in its operand, they are all enclosed by the pair of brackets appearing immediately after the product sign.) Consider the base case of the induction where $K = 1$. There exists an unordered pair of taxa $\{w^*, z^*\}$ such that $\{W_1, Z_1\} = \{\{w^*\}, \{z^*\}\}$. The probability density $q_{\phi,1}(\tau_{1:1}, \mathbf{t}_{1:1})$ is the density of the event that taxa w^* and z^* coalesce at time t_1 ($q_{\phi}^{\{w^*, z^*\}}(t_1)$) times the probability that all other taxa coalesce after time t_1 (as $\{W_1, Z_1\}$ is the first bipartition). Therefore, we have:

$$q_{\phi,1}(\tau_{1:1}, \mathbf{t}_{1:1}) = q_{\phi}^{\{w^*, z^*\}}(t_1) \prod_{\{w,z\} \neq \{w^*, z^*\}} Q_{\phi}^{\{w,z\}}(t_1) \quad (13)$$

$$= \frac{q_{\phi}^{\{w^*, z^*\}}(t_1)}{Q_{\phi}^{\{w^*, z^*\}}(t_1)} Q_{\phi}^{\{w^*, z^*\}}(t_1) \prod_{\{w,z\} \notin \mathcal{S}_1} Q_{\phi}^{\{w,z\}}(t_1). \quad (14)$$

$$= \left(\sum_{\{w,z\} \in \mathcal{S}_1} \frac{q_{\phi}^{\{w,z\}}(t_1)}{Q_{\phi}^{\{w,z\}}(t_1)} \right) \left(\prod_{\{w,z\} \in \mathcal{S}_1} Q_{\phi}^{\{w,z\}}(t_1) \right) \prod_{\{w,z\} \notin \mathcal{S}_{1:1}} Q_{\phi}^{\{w,z\}}(t_1). \quad (15)$$

Here in (13) we use the mutual independence of $t^{(\cdot,\cdot)}$ to split the joint probability of all taxa other than $\{w^*, z^*\}$ coalescing after t_1 into a product. Thus, the base case ($K = 1$) is established. Assume that the induction hypothesis (12) holds for a given $K - 1$ (here $1 \leq K - 1 < N - 1$). Consider the conditional probability density function $q_{\phi,K}(\{W_K, Z_K\}, t_K \mid \tau_{1:K-1}, \mathbf{t}_{1:K-1})$. When we condition on $\tau_{1:K-1}, \mathbf{t}_{1:K-1}$, the K -th coalescent event with bipartition $\{W_K, Z_K\}$ occurs at time t_K if and only if the following hold:

1. There exists an unordered pair of taxa $\{w^*, z^*\} \in \mathcal{S}(W_K, Z_K)$ such that $t^{\{w^*, z^*\}} = t_K$. (We are conditioning on the event that taxa w^* and z^* have not coalesced before time t_{K-1} .) The conditional probability density of the event that w^* and z^* coalesce at time t_K is thus $q_{\phi}^{\{w^*, z^*\}}(t_K)/Q_{\phi}^{\{w^*, z^*\}}(t_{K-1})$.
2. All *other* taxa pairs that have not coalesced by time t_{K-1} coalesce after time t_K . (As the $q_{\phi}^{\{\cdot,\cdot\}}$'s are continuously differentiable, they are continuous and so $\{w^*, z^*\}$ is unique almost surely.) Note that we are conditioning on the event that all taxa pairs $\{w, z\} \notin \mathcal{S}_{1:K-1}$ have not coalesced before time t_{K-1} . The conditional probability density of the event that w^* and z^* have not coalesced by time t_K is thus $Q_{\phi}^{\{w^*, z^*\}}(t_K)/Q_{\phi}^{\{w^*, z^*\}}(t_{K-1})$.

The conditional probability density is thus:

$$q_{\phi,K}(\{W_K, Z_K\}, t_K \mid \tau_{1:K-1}, \mathbf{t}_{1:K-1}) \quad (16)$$

$$= \sum_{\{w^*, z^*\} \in \mathcal{S}_K} \left(\frac{q_{\phi}^{\{w^*, z^*\}}(t_K)}{Q_{\phi}^{\{w^*, z^*\}}(t_{K-1})} \prod_{\substack{\{w, z\} \notin \mathcal{S}_{1:K-1} \\ \{w, z\} \neq \{w^*, z^*\}}} \frac{Q_{\phi}^{\{w, z\}}(t_K)}{Q_{\phi}^{\{w, z\}}(t_{K-1})} \right) \quad (17)$$

$$= \left(\sum_{\{w, z\} \in \mathcal{S}_K} \frac{q_{\phi}^{\{w, z\}}(t_K)}{Q_{\phi}^{\{w, z\}}(t_K)} \right) \prod_{\{w, z\} \notin \mathcal{S}_{1:K-1}} \frac{Q_{\phi}^{\{w, z\}}(t_K)}{Q_{\phi}^{\{w, z\}}(t_{K-1})} \quad (18)$$

$$= \left(\sum_{\{w, z\} \in \mathcal{S}_K} \frac{q_{\phi}^{\{w, z\}}(t_K)}{Q_{\phi}^{\{w, z\}}(t_K)} \right) \left(\prod_{\{w, z\} \in \mathcal{S}_K} \frac{Q_{\phi}^{\{w, z\}}(t_K)}{Q_{\phi}^{\{w, z\}}(t_{K-1})} \right) \prod_{\{w, z\} \notin \mathcal{S}_{1:K}} \frac{Q_{\phi}^{\{w, z\}}(t_K)}{Q_{\phi}^{\{w, z\}}(t_{K-1})}. \quad (19)$$

Note that we drop the stars on the taxa w and z after (17) because the indices no longer need to be distinguished once the sum is isolated. Also, in (17) we use the mutual independence of $t^{(\cdot,\cdot)}$ to form the product. Multiplying this conditional probability with the induction hypothesis (12) for $K - 1$ yields the total probability density:

$$q_{\phi,K}(\tau_{1:K}, \mathbf{t}_{1:K}) = q_{\phi,K}(\{W_K, Z_K\}, t_K \mid \tau_{1:K-1}, \mathbf{t}_{1:K-1}) \cdot q_{\phi,K-1}(\tau_{1:K-1}, \mathbf{t}_{1:K-1}) \quad (20)$$

$$= \left(\sum_{\{w, z\} \in \mathcal{S}_K} \frac{q_{\phi}^{\{w, z\}}(t_K)}{Q_{\phi}^{\{w, z\}}(t_K)} \right) \left(\prod_{\{w, z\} \in \mathcal{S}_K} \frac{Q_{\phi}^{\{w, z\}}(t_K)}{Q_{\phi}^{\{w, z\}}(t_{K-1})} \right) \left(\prod_{\{w, z\} \notin \mathcal{S}_{1:K}} \frac{Q_{\phi}^{\{w, z\}}(t_K)}{Q_{\phi}^{\{w, z\}}(t_{K-1})} \right) \quad (21)$$

$$\cdot \prod_{n=1}^{K-1} \left(\left(\sum_{\{w, z\} \in \mathcal{S}_n} \frac{q_{\phi}^{\{w, z\}}(t_n)}{Q_{\phi}^{\{w, z\}}(t_n)} \right) \prod_{\{w, z\} \in \mathcal{S}_n} Q_{\phi}^{\{w, z\}}(t_n) \right) \prod_{\{w, z\} \notin \mathcal{S}_{1:K-1}} Q_{\phi}^{\{w, z\}}(t_{K-1}). \quad (22)$$

We then move the first component of line (21) into the first component of line (22), and we move the numerator of the second component of line (21) into the second component of line (22). These rearrangements yield the following:

$$q_{\phi,K}(\tau_{1:K}, \mathbf{t}_{1:K}) = \left(\prod_{\{w,z\} \in \mathcal{S}_K} \frac{1}{Q_{\phi}^{\{w,z\}}(t_{K-1})} \right) \left(\prod_{\{w,z\} \notin \mathcal{S}_{1:K}} \frac{Q_{\phi}^{\{w,z\}}(t_K)}{Q_{\phi}^{\{w,z\}}(t_{K-1})} \right) \\ \cdot \prod_{n=1}^K \left(\left(\sum_{\{w,z\} \in \mathcal{S}_n} \frac{q_{\phi}^{\{w,z\}}(t_n)}{Q_{\phi}^{\{w,z\}}(t_n)} \right) \prod_{\{w,z\} \in \mathcal{S}_n} Q_{\phi}^{\{w,z\}}(t_n) \right) \prod_{\{w,z\} \notin \mathcal{S}_{1:K-1}} Q_{\phi}^{\{w,z\}}(t_{K-1}). \quad (23)$$

For the final display, in (24) we split the numerator and denominator of $\frac{Q_{\phi}^{\{w,z\}}(t_K)}{Q_{\phi}^{\{w,z\}}(t_{K-1})}$ into separate products. And in (25) we cancel the $Q_{\phi}^{\{w,z\}}(t_{K-1})$ factors involving $\{w, z\} \in \mathcal{S}_K$. And in (26) we cancel the $Q_{\phi}^{\{w,z\}}(t_{K-1})$ factors involving $\{w, z\} \notin \mathcal{S}_{1:K-1}$.

$$q_{\phi,K}(\tau_{1:K}, \mathbf{t}_{1:K}) = \left(\prod_{\{w,z\} \in \mathcal{S}_K} \frac{1}{Q_{\phi}^{\{w,z\}}(t_{K-1})} \right) \left(\prod_{\{w,z\} \notin \mathcal{S}_{1:K}} \frac{1}{Q_{\phi}^{\{w,z\}}(t_{K-1})} \right) \left(\prod_{\{w,z\} \notin \mathcal{S}_{1:K}} Q_{\phi}^{\{w,z\}}(t_K) \right) \\ \cdot \prod_{n=1}^K \left(\left(\sum_{\{w,z\} \in \mathcal{S}_n} \frac{q_{\phi}^{\{w,z\}}(t_n)}{Q_{\phi}^{\{w,z\}}(t_n)} \right) \prod_{\{w,z\} \in \mathcal{S}_n} Q_{\phi}^{\{w,z\}}(t_n) \right) \prod_{\{w,z\} \notin \mathcal{S}_{1:K-1}} Q_{\phi}^{\{w,z\}}(t_{K-1}) \quad (24)$$

$$= \left(\prod_{\{w,z\} \notin \mathcal{S}_{1:K-1}} \frac{1}{Q_{\phi}^{\{w,z\}}(t_{K-1})} \right) \left(\prod_{\{w,z\} \notin \mathcal{S}_{1:K}} Q_{\phi}^{\{w,z\}}(t_K) \right) \\ \cdot \prod_{n=1}^K \left(\left(\sum_{\{w,z\} \in \mathcal{S}_n} \frac{q_{\phi}^{\{w,z\}}(t_n)}{Q_{\phi}^{\{w,z\}}(t_n)} \right) \prod_{\{w,z\} \in \mathcal{S}_n} Q_{\phi}^{\{w,z\}}(t_n) \right) \prod_{\{w,z\} \notin \mathcal{S}_{1:K-1}} Q_{\phi}^{\{w,z\}}(t_{K-1}) \quad (25)$$

$$= \prod_{n=1}^K \left(\left(\sum_{\{w,z\} \in \mathcal{S}_n} \frac{q_{\phi}^{\{w,z\}}(t_n)}{Q_{\phi}^{\{w,z\}}(t_n)} \right) \prod_{\{w,z\} \in \mathcal{S}_n} Q_{\phi}^{\{w,z\}}(t_n) \right) \prod_{\{w,z\} \notin \mathcal{S}_{1:K}} Q_{\phi}^{\{w,z\}}(t_K). \quad (26)$$

Thus, the inductive step is established and (12) holds for all $1 \leq K \leq N - 1$. To complete the derivation, note that $q_{\phi,N-1} = q_{\phi}$; and $\mathcal{S}_{1:N-1} = \bigcup_{n=1}^{N-1} \mathcal{S}(W_n, Z_n) = \{\{w, z\} : w, z \in \mathcal{X}\}$ (all taxa coalesce after $N - 1$ coalescent events); and indices over $w \in W_n, z \in Z_n$ are equivalent to indices over $\{w, z\} \in \mathcal{S}_n$. Thus, for $K = N - 1$ the last

term of (26) is an empty product yielding the desired result:

$$q_\phi(\tau, \mathbf{t}) = q_{\phi, N-1}(\tau_{1:N-1}, \mathbf{t}_{1:N-1}) \quad (27)$$

$$= \prod_{n=1}^{N-1} \left(\left(\sum_{\{w,z\} \in \mathcal{S}_n} \frac{q_\phi^{\{w,z\}}(t_n)}{Q_\phi^{\{w,z\}}(t_n)} \right) \prod_{\{w,z\} \in \mathcal{S}_n} Q_\phi^{\{w,z\}}(t_n) \right) \quad (28)$$

$$= \prod_{n=1}^{N-1} \left(\left(\sum_{\substack{w \in W_n \\ z \in Z_n}} \frac{q_\phi^{\{w,z\}}(t_n)}{Q_\phi^{\{w,z\}}(t_n)} \right) \prod_{\substack{w \in W_n \\ z \in Z_n}} Q_\phi^{\{w,z\}}(t_n) \right). \quad (29)$$

Appendix B: Additional Results

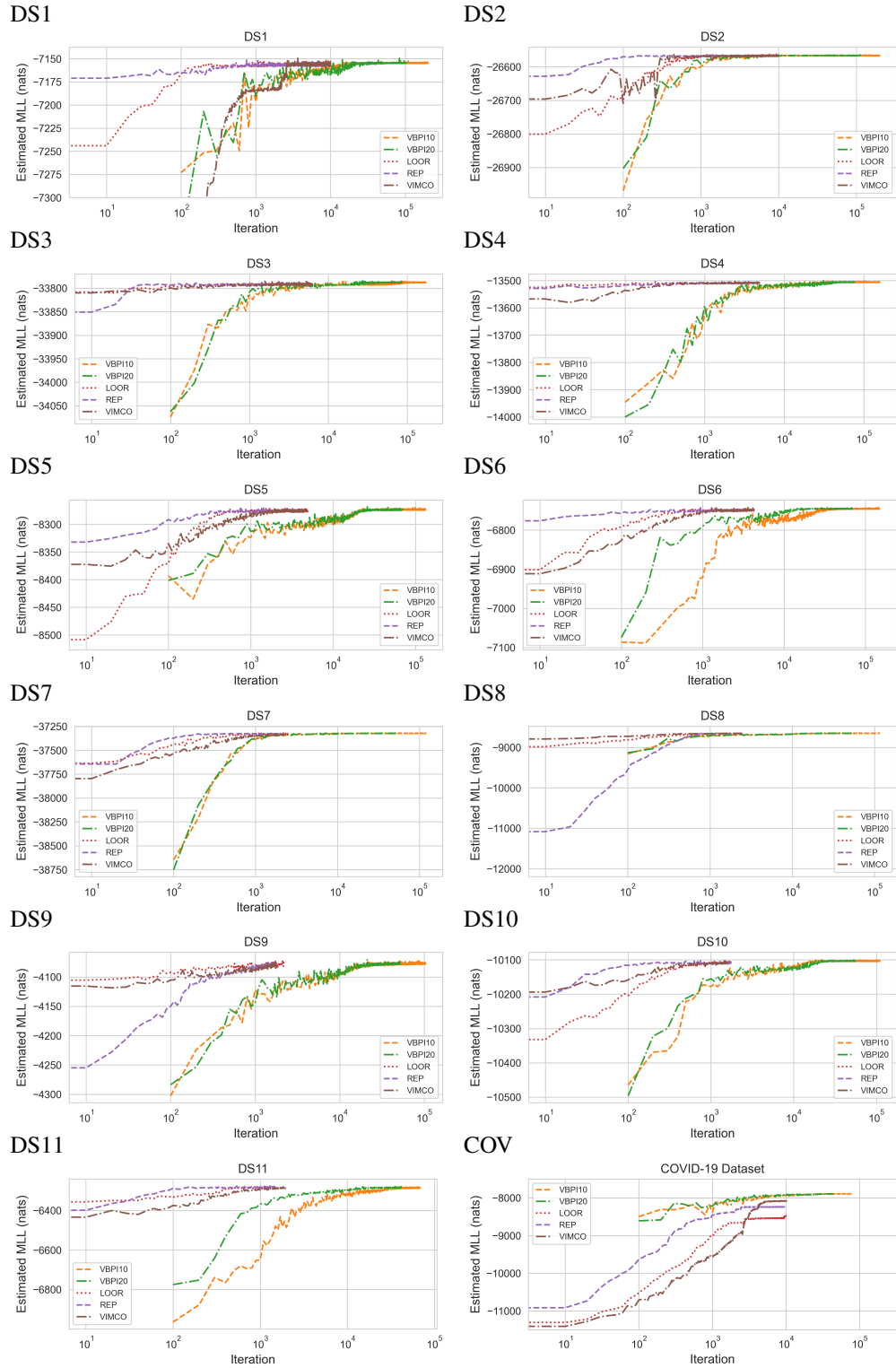


Figure 5: *Trace plots for all datasets.* Trace plot of estimated marginal log-likelihood vs. iteration number (i.e., parameter update number). Marginal log-likelihood was estimated using 500 importance samples for VBPI and 50 importance samples for VIPR methods.

Appendix C: Gradient Estimators for q_ϕ

C.1 REINFORCE Estimator

Define $f_\phi(\tau, \mathbf{t}) \equiv \log(p(\tau, \mathbf{t}, \mathbf{Y}^{(\text{ob})})) - \log(q_\phi(\tau, \mathbf{t}))$, so that $L(\phi) = \mathbb{E}_{q_\phi}[f_\phi(\tau, \mathbf{t})]$. We can interchange the gradients and the finite sum over τ due to the linearity of integrals. Further, conditioned on τ , the integrand in Equation (7) is continuously differentiable in both ϕ and \mathbf{t} , so we can interchange the gradient and the integral from Equation (7). After performing some algebra, we obtain the *leave-one-out REINFORCE* (LOOR) estimator (Mnih and Gregor, 2014; Shi et al., 2022):

$$\nabla_\phi L(\phi) \approx \frac{1}{K} \sum_{k=1}^K w^{(k)} \nabla_\phi \log q_\phi(\tau^{(k)}, \mathbf{t}^{(k)}), \quad (30)$$

$$w^{(k)} = f_\phi(\tau^{(k)}, \mathbf{t}^{(k)}) - \hat{f}^{(-k)}, \quad (31)$$

$$\hat{f}^{(-k)} = \frac{1}{K-1} \sum_{\ell \neq k} f_\phi(\tau^{(\ell)}, \mathbf{t}^{(\ell)}) \quad (32)$$

$$(\tau^{(k)}, \mathbf{t}^{(k)}) \sim q_\phi. \quad (33)$$

The gradient $\nabla_\phi \log q_\phi(\tau^{(k)}, \mathbf{t}^{(k)})$ can be calculated using automatic differentiation software such as Autograd (Maclaurin et al., 2015) or PyTorch (Paszke et al., 2019).

C.2 The Reparameterization Trick

The *reparameterization trick* applied in our experiments when $q_\phi^{\{u,v\}}$ is a log-normal distribution for all u and $v \in \mathcal{X}$. In Algorithm (2), the candidate coalescent times $t^{\{u,v\}} \sim \text{Lognormal}(\mu^{\{u,v\}}, \sigma^{\{u,v\}}) \iff t^{\{u,v\}} = \exp(\mu^{\{u,v\}} + \sigma^{\{u,v\}} z^{\{u,v\}})$ with $z^{\{u,v\}} \sim \mathcal{N}(0, 1)$. Thus, we reparameterize the expectation in Equation (6) as follows:

$$L(\phi) = \mathbb{E}_{\mathbf{Z}} \left[\log \left(\frac{p(\mathbf{Y}, g_\phi(\mathbf{Z}))}{q_\phi(g_\phi(\mathbf{Z}))} \right) \right]. \quad (34)$$

Where $g_\phi(\mathbf{Z}) = \text{Single-Linkage Clustering}(\exp(\boldsymbol{\mu} + \boldsymbol{\sigma} \odot \mathbf{Z}), \mathcal{X})$. Denoting the multivariate standard normal density as $\mathcal{N}(\cdot; \mathbf{0}, I)$, we have

$$L(\phi) = \int_{\mathbf{Z}} \mathcal{N}(\mathbf{Z}; \mathbf{0}, I) \log \left(\frac{p(\mathbf{Y}, g_\phi(\mathbf{Z}))}{q_\phi(g_\phi(\mathbf{Z}))} \right) d\mathbf{Z}. \quad (35)$$

However, the denominator $q_\phi(g_\phi(\mathbf{Z}))$ has jump discontinuities with respect to ϕ and \mathbf{Z} because the tree structure τ is discrete. Therefore, we cannot interchange the integral and the gradient when estimating the full gradient. Instead, we sum over the tree structures τ and then integrate over $\mathbb{Z}_\tau(\phi)$, the space of all values of \mathbf{Z} that are consistent with that tree structure given the parameters ϕ :

$$L(\phi) = \sum_{\tau} \int_{\mathbf{Z} \in \mathbb{Z}_\tau(\phi)} \mathcal{N}(\mathbf{Z}; \mathbf{0}, I) \log \left(\frac{p(\mathbf{Y}, g_\phi(\mathbf{Z}))}{q_\phi(g_\phi(\mathbf{Z}))} \right) d\mathbf{Z}. \quad (36)$$

Then, the gradient can be approximated as follows:

$$\nabla_\phi L(\phi) \approx \mathbb{E}_{\mathbf{Z}} \left[\nabla_\phi \log \left(\frac{p(\mathbf{Y}, g_\phi(\mathbf{Z}))}{q_\phi(g_\phi(\mathbf{Z}))} \right) \right]. \quad (37)$$

We note that this is an approximation because the region of integration itself depends upon ϕ , which adds additional terms into the interchange of the integral and the gradient. Nonetheless, we still define a *biased* estimate of $\nabla_\phi L(\phi)$ as

$$\widehat{\nabla}_\phi L(\phi) \approx \frac{1}{K} \sum_{k=1}^K \nabla_\phi \log \left(\frac{p(\mathbf{Y}, g_\phi(\mathbf{Z}^{(k)}))}{q_\phi(g_\phi(\mathbf{Z}^{(k)}))} \right) \quad (38)$$

$$\mathbf{Z}^{(k)} \sim \mathcal{N}(\cdot; \mathbf{0}, I). \quad (39)$$

As with the LOOR estimator, the gradient $\nabla_{\phi} \log \left(\frac{p(\mathbf{Y}, g_{\phi}(\mathbf{Z}^{(k)}))}{q_{\phi}(g_{\phi}(\mathbf{Z}^{(k)}))} \right)$ can be calculated using automatic differentiation software such as Autograd (Maclaurin et al., 2015) or PyTorch (Paszke et al., 2019). Because this estimate is not unbiased, it is not guaranteed to converge to a local optimum of the objective function. Nonetheless, these gradient estimates perform at least comparably to the LOOR estimator.

C.3 The VIMCO Estimator

When using the K -sample ELBO objective from Equation (11), the VIMCO estimator is an analogous gradient estimator to the LOOR estimator for the single-sample ELBO:

$$\nabla_{\phi} L_K(\phi) \approx \sum_{k=1}^K \left(\hat{L}_K^{(-k)}(\phi) - \tilde{w}^{(k)} \right) \nabla_{\phi} \log q_{\phi}(\tau^{(k)}, \mathbf{t}^{(k)}) \quad (40)$$

$$\tilde{w}^{(k)} = \frac{f_{\phi}(\tau^{(k)}, \mathbf{t}^{(k)})}{\sum_{\ell=1}^K f_{\phi}(\tau^{(\ell)}, \mathbf{t}^{(\ell)})} \quad (41)$$

$$\hat{L}_K^{(-k)}(\phi) = \hat{L}_K(\phi) - \log \frac{1}{K} \left(\sum_{\ell \neq k} f_{\phi}(\tau^{(\ell)}, \mathbf{t}^{(\ell)}) + \hat{f}_{\phi}^{(-\ell)} \right) \quad (42)$$

$$\hat{L}_K(\phi) = \log \left(\frac{1}{K} \sum_{k=1}^K f_{\phi}(\tau^{(k)}, \mathbf{t}^{(k)}) \right) \quad (43)$$

$$\hat{f}_{\phi}^{(-\ell)} = \frac{1}{K-1} \sum_{j \neq \ell} f_{\phi}(\tau^{(j)}, \mathbf{t}^{(j)}) \quad (44)$$

$$(\tau^{(k)}, \mathbf{t}^{(k)}) \sim q_{\phi}. \quad (45)$$